Chem Catalysis

CellPress

Article

Water-assisted shape-selective production of ethene in methanol-to-olefins reaction on SAPO-34

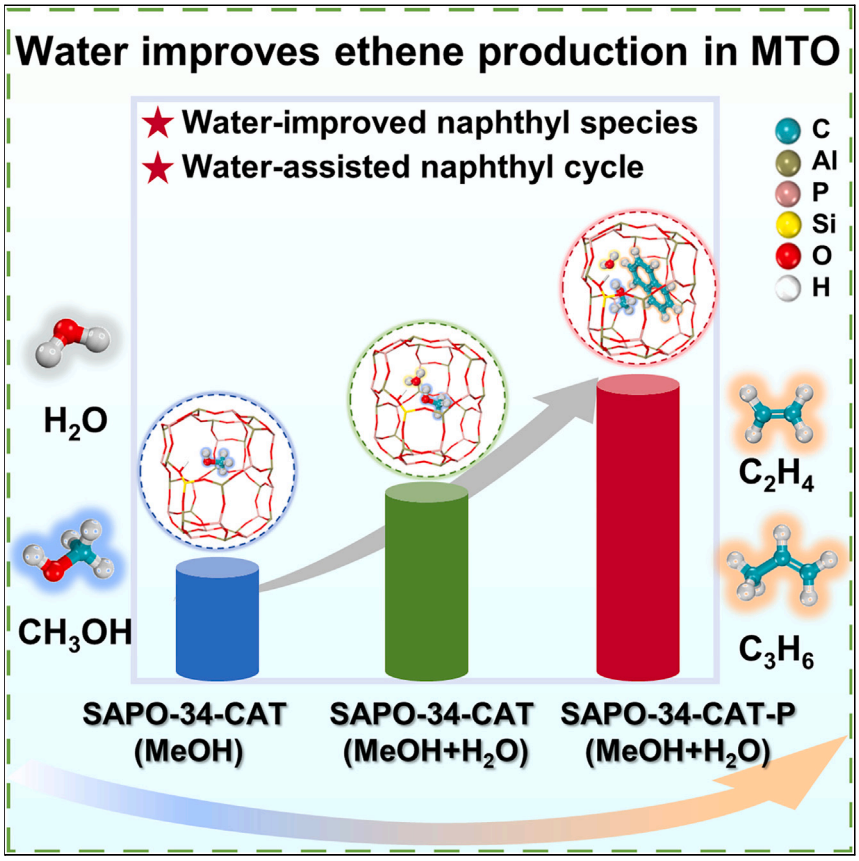

As a critical issue in zeolite catalysis, the role of water in the methanol-to-olefins (MTO) reaction has attracted tremendous attention from academia and industry. By combining multiple experimental techniques and theoretical calculations, we have elucidated the mechanistic role of water in inducing a higher concentration of naphthyl species and promoting the naphthyl-based catalytic reaction cycle, leading to an enhancement of ethene selectivity.

Chengwei Zhang, Xinqiang Wu, Yanan Zhang, ..., Liang Wang, Yingxu Wei, Zhongmin Liu

weiyx@dicp.ac.cn (Y.W.)
liuzm@dicp.ac.cn (Z.L.)

Highlights

Cofeeding water in the MTO reaction over SAPO-34 obtained an ethene selectivity of 57.7%

Water cofeeding improved the concentration and reactivity of naphthyl species

Water participation decreased the reaction energy barrier for ethene formation

Cofeeding water in a naphthyl-species catalyst gained an ethene selectivity of 67.5%

Zhang et al., Chem Catalysis 4, 101025
July 18, 2024 © 2024 Elsevier Inc. All rights are reserved, including those for text and data mining, AI training, and similar technologies.
https://doi.org/10.1016/j.checat.2024.101025

Please cite this article in press as: Zhang et al., Water-assisted shape-selective production of ethene in methanol-to-olefins reaction on SAPO-34, Chem Catalysis (2024), https://doi.org/10.1016/j.checat.2024.101025

Chem Catalysis

CellPress

Article

Water-assisted shape-selective production of ethene in methanol-to-olefins reaction on SAPO-34

Chengwei Zhang,[1,4] Xinqiang Wu,[1] Yanan Zhang,[1,4] Wenna Zhang,[1] Shanfan Lin,[1] Caiyi Lou,[1,4] Shutao Xu,[1] Dawei He,[3] Liang Wang,[3] Yingxu Wei,[1,*] and Zhongmin Liu[1,2,4,5,*]

SUMMARY

Comprehending the role of water in the methanol-to-olefins (MTO) reaction is of utmost importance. Herein, we report an unprecedented ethene selectivity of approximately 58% with water assistance during the MTO reaction over SAPO-34, along with an extension of catalyst lifespan. The *in situ* spectroscopic observations and isotope switching experiments revealed that naphthyl species with higher concentration were retained in SAPO-34 and exhibited higher reactivity when cofeeding water with methanol. The density functional theory calculations suggested that the water-mediated microenvironment not only activates the methanol molecules but also serves as a proton transfer reagent between the zeolite framework and the organic intermediates, contributing to a lower reaction energy barrier for ethene formation. A strategy of cofeeding water with methanol over a naphthyl-species pre-accommodated SAPO-34 catalyst is proposed, achieving an enhanced ethene selectivity up to 67.5%. The mechanistic insights and strategy development deepen the understanding of the role of water in zeolite catalysis and offer optimizations for MTO industrial applications.

INTRODUCTION

The structure and dynamic behavior of water have been the subjects of significant interest in the fields of materials science,[1] energy,[2] catalysis,[3] etc. In the catalytic reaction system, water is commonly present as a reactant, product, or reaction medium, which can affect the catalyst material and catalytic performance. For example, the catalyst's material surface was hampered by water and thus induced deactivation in the Fischer-Tropsch synthesis process,[4] but this can be suppressed by shifting the water-sorption equilibrium on the catalyst's surface.[5] Water can also improve the reaction rate by directly participating in the reaction pathway by dissociating itself[6] or creating an ionic environment by forming hydronium ions.[7] It is increasingly recognized that the presence of water can affect both the thermodynamic state and the kinetic process of the catalytic reaction system, with potential influence on the adsorption and diffusion of chemical molecules on catalysts through the regulation of surface structure and physical and chemical properties. Therefore, gaining insights into the role of water in catalytic reaction systems will provide theoretical knowledge and reference for the application and development of water in the field of catalysis.

In heterogeneous catalytic transformations involving oxygen-containing compounds (e.g., alcohol, CO, CO_2, and biomass), water is often inevitable. In the typical

THE BIGGER PICTURE

The role of water in the methanol-to-olefins (MTO) reaction for promoting ethene formation over SAPO-34 was revealed. Water cofeeding induced a higher concentration of naphthyl species in SAPO-34 and promoted the catalytic reaction cycle with naphthyl species, resulting in an increase of ethene selectivity from 49.7% to 57.7%. Based on this knowledge, the strategy of cofeeding water with methanol over a naphthyl-species pre-accommodated SAPO-34 catalyst was proposed to achieve a high ethene selectivity of 67.5%. This work provides a deeper insight into the role of water in catalytic reactions and will provide theoretical knowledge and reference for catalysis in the atmosphere of water.

All rights are reserved, including those for text and data mining, AI training, and similar technologies.

Please cite this article in press as: Zhang et al., Water-assisted shape-selective production of ethene in methanol-to-olefins reaction on SAPO-34, Chem Catalysis (2024), https://doi.org/10.1016/j.checat.2024.101025

case of the methanol-to-olefins (MTO) reaction over a zeolite catalyst, water not only acts as a stoichiometric by-product in methanol conversion[8–10] but also functions as a cofeed or atmosphere component, primarily regulating the heat transfer. In fact, researchers have recognized that water can greatly influence the framework of zeolite materials as well as the physicochemical properties of the catalytic interface, adsorption, and diffusion processes, thereby affecting the MTO reaction performance. Lercher and colleagues discovered that water molecules interacted with the protons in Brønsted acid sites (BASs), forming water clusters or hydronium ions that occupy the acid sites and inhibit the adsorption of reactant molecules on BASs.[11–14] Our previous work found that the dynamic and reversible breaking of the T–O–T bonds of the zeolite framework can be achieved by water hydrolysis under mild hydrothermal conditions, as observed through spectroscopy and isotope tracing techniques.[15] Dai and coworkers indicated that long-term interaction with water in the MTO reaction led to the irreversible breakage of T–O–T bonds and partial framework collapse of the catalyst.[16] In addition, Bert M. Weckhuysen and colleagues revealed that water molecules enhanced the zeolite crystal utilization efficiency, thereby facilitating the diffusion of methanol and small reactive molecules into the interior of the zeolite crystals.[17] Although the introduction of water has been observed to reduce the coke deposition rate, prolong the catalyst lifespan, and improve the alkene products selectivity to some extent in the MTO reaction,[18–24] the intricate mechanisms involving the water-mediated dynamic catalytic process of the MTO reaction remain elusive.

The MTO reaction over zeolite catalysts typically goes through three stages: induction, high efficiency, and deactivation.[8–10,25–28] In the initial stage of the induction period, the first carbon–carbon (C–C) bond forms via a direct mechanism,[29–32] followed by the formation and transformation of initial olefins.[33,34] Gradually, the hydrocarbon pool (HCP) is established based on olefinic-based and/or aromatic-based species, promoting the efficient conversion of methanol to hydrocarbons via the HCP mechanism.[35–37] Ultimately, with the formation and growth of polycyclic aromatic hydrocarbons (PAHs), the catalytic reaction exhibits a trend of conversion decline or even deactivation.[38–41] Water is always present in this dynamic catalytic process and may influence the reaction at different periods by regulating the catalytic interface, reaction intermediates, transition states (TSs), and so on. As demonstrated by molecular simulations and experimental evidence, the presence of water reduces the methanol reactivity and leads to a prolonged induction period for HCP intermediate formation.[17] Moreover, water could also directly participate in the elemental steps by acting as a proton transfer reagent to assist the deprotonation and olefin elimination in the highly efficient methanol conversion period.[42–47] In the deactivation stage, water suppresses PAH clustering,[41] reducing the coke deposition rate and leading to the extension of the catalyst's lifespan. More importantly, recent works have well elucidated that water can serve as a regeneration atmosphere to realize an incomplete regeneration of deactivated catalyst by *in situ* decomposition of the cross-linked cage-passing PAHs at relatively high temperature.[41,48,49] However, the existing understanding of water's participation and regulation in the MTO reaction mostly relies on empirical observations and catalytic phenomenon reports. Achieving a comprehensive, molecular-level mechanistic understanding is imperative to elucidate the precise role of water in the MTO reaction over a zeolite catalyst.

In the present work, cofeeding of water was conducted in methanol conversion, and an unprecedented ethene selectivity of approximately 58%, along with catalyst lifetime extension, was observed in the MTO reaction over SAPO-34. The role of water in promoting ethene formation was experimentally revealed by the aid of gas

[1]National Engineering Research Center of Lower-Carbon Catalysis Technology, Dalian National Laboratory for Clean Energy, iChEM (Collaborative Innovation Center of Chemistry for Energy Materials), Dalian Institute of Chemical Physics, Chinese Academy of Sciences, Dalian 116023, China

[2]State Key Laboratory of Catalysis, Dalian Institute of Chemical Physics, Chinese Academy of Sciences, Dalian 116023, China

[3]Catalyst & Catalysis Technology Co. Ltd. of CAS, Dalian 116023, China

[4]University of Chinese Academy of Sciences, Beijing 100049, China

[5]Lead contact

*Correspondence: weiyx@dicp.ac.cn (Y.W.), liuzm@dicp.ac.cn (Z.L.)

https://doi.org/10.1016/j.checat.2024.101025

Please cite this article in press as: Zhang et al., Water-assisted shape-selective production of ethene in methanol-to-olefins reaction on SAPO-34, Chem Catalysis (2024), https://doi.org/10.1016/j.checat.2024.101025

chromatography-mass spectrometry (GC-MS), *in situ* UV-visible (UV-vis) spectroscopy, and $^{12}C/^{13}C$-CH_3OH switch experiments. Water cofeeding gave rise to increased concentration of deposited naphthyl species in the SAPO-34 chabazite (CHA) cages and improved the activity of naphthyl species toward methanol conversion as HCP species. Complementing experimental observations, density functional theory (DFT) calculations uncovered the role of water in promoting the naphthyl-based catalytic reaction cycle by aiding methanol pre-activation and serving as the bridge for proton transport between zeolite and organic intermediates. An energetically favorable route was demonstrated by DFT calculations for ethene formation via the naphthyl-based catalytic reaction cycle with water assistance. Based on the experimental and theoretical studies, water-promoted ethene-selective production in the MTO reaction has been elucidated, and the molecular-level mechanistic insights also contribute to an in-depth understanding of the role of water in zeolite catalysis. Further enhancement of ethene selectivity was achieved through the synergistic strategy of cofeeding water with methanol over the SAPO-34 catalyst (SAPO-34-CAT) pre-conditioned with naphthyl species.

RESULTS AND DISCUSSION

MTO reaction under the condition of water cofeeding over SAPO-34

The characterization results of SAPO-34 are shown in Figure S1 and Table S1. The X-ray diffraction (XRD) pattern indicates a good crystallinity with the CHA structure (Figure S1A). SAPO-34 shows a Si content of 0.0875 (Si/(Si + Al + P), molar ratio). Scanning electron microscope (SEM) exhibits relatively uniform cubic crystal particles with particle size of 8 μm (Figure S1B). ^{1}H and ^{29}Si magic-angle spinning (MAS) NMR spectroscopy demonstrates the sole Si(4Al) environment of SAPO-34 with BASs (Figures S1C and S1D).

The cofeeding of water and methanol can help to extend the catalyst's lifetime and improve the olefin selectivity in MTO conversion.[18–20] The competitive adsorption of water has been proposed as a reasonable explanation for depressing the access of reactants and products to active acidic sites and the occurrence of secondary reactions.[17] The effect of water on the MTO reaction needs to be considered in the context of the actual reaction conditions, e.g., reaction temperature[50] and pressure.[22,23] Herein, the influences of water on methanol conversion and product selectivity on SAPO-34 were investigated at 623 and 773 K with a methanol weight hourly space velocity (WHSV) of 2 h^{-1} (Figure 1). At the low reaction temperature of 623 K, an induction period of incomplete methanol conversion was observed in water cofeeding reactions (Figure 1A). Furthermore, this induction period was more pronounced with increasing water content from 1:0 to 1:6 (methanol/water [molar ratio]). On one hand, this was attributed to the direct competition of water adsorption at active sites and the resulting decrease in the available sites for methanol conversion at the low reaction temperature. On the other hand, the presence of water inhibited the efficient formation of HCP species at the beginning of the reaction, leading to insufficient conversion of methanol during the initial reaction stage, which was consistent with previous research conclusions.[17,24,41] Interestingly, the product selectivity and E/P (ethene/propene) ratio remained almost unchanged under the water cofeeding condition (Figures 1B and S2). Before the occurrence of catalyst deactivation, the catalyst's lifespan for low-temperature methanol conversion was almost the same, even for methanol conversion when cofeeding water at different methanol/water ratios. Therefore, it can be speculated that cofeeding water at low reaction temperature can reduce the methanol conversion efficiency through competitive adsorption and other effects at the beginning of the reaction,

Please cite this article in press as: Zhang et al., Water-assisted shape-selective production of ethene in methanol-to-olefins reaction on SAPO-34, Chem Catalysis (2024), https://doi.org/10.1016/j.checat.2024.101025

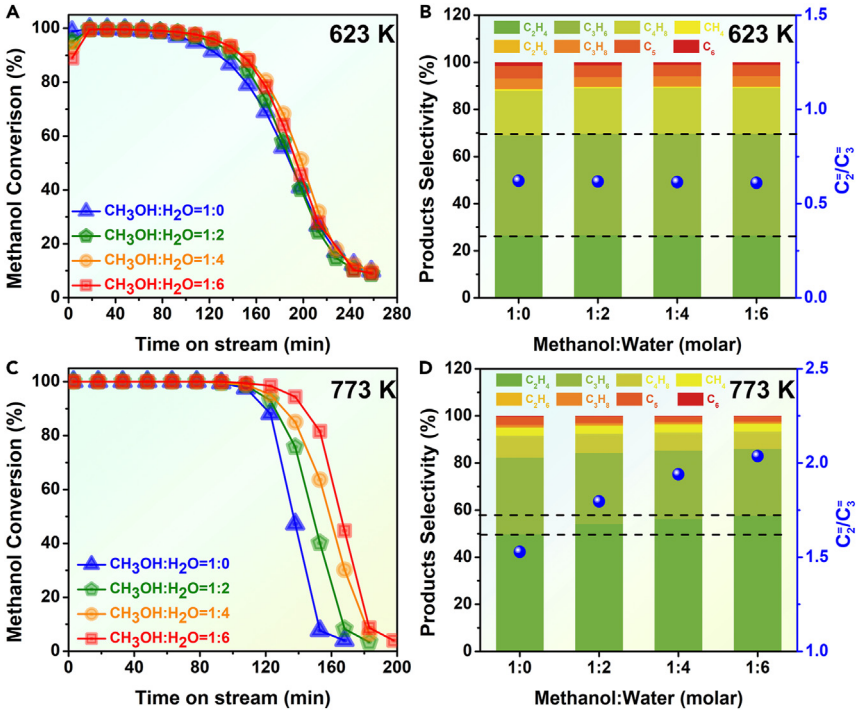

Figure 1. Catalytic performance in the MTO reaction under the condition of water cofeeding over SAPO-34 with a WHSV of 2 h^{-1} at different water contents

(A) Methanol conversion at 623 K.

(B) Product selectivity at 623 K.

(C) Methanol conversion at 773 K.

(D) Product selectivity at 773 K.

but it does not significantly alter the reaction pathway of methanol conversion nor light olefin generation during the highly reactive period and the deactivation period under the mild reaction conditions of low reaction temperature.

Contrasting with the reaction at low temperature, the induction period of the MTO reaction was almost undetectable at the higher temperature of 773 K (Figure 1C), even with an increased water content from 1:0 to 1:6 (methanol/water [molar ratio]). This indicates that the competitive adsorption of water is weakened or eliminated at high temperature, and the retarded effect on the formation of HCP species is greatly reduced in this way. Notably, the MTO performance was even promoted by cofeeding water on SAPO-34 to some extent, mainly manifested in the extension of the duration of complete methanol conversion from 80 to 110 min (Figure 1C) and the increase of C_2-C_4 olefin selectivity from 91.1% to 92.6% (Figure S3). However, the surprising result was that ethene and other olefin products showed a marked difference in selectivity. Specifically, an obvious improvement in ethene selectivity from 49.7% to 57.7% was observed when the water content increased from 1:0 to 1:6, while the propene selectivity decreased from 32.5% to 28.3% and the corresponding E/P ratio increased from 1.5 to 2.0 (Figure 1D). Furthermore, the butene selectivity also decreased from 9.3% to 7.4% (Figure S3). Lercher and coworkers reported that the adsorption of water on zeolite materials with the form of water clusters became disordered and mobile, inducing a quick proton exchange among water molecules and acid sites with temperature increase.[11] For MTO reactions conducted at 773 K, the high temperature weakened and eliminated the competitive adsorption of water on acidic sites. However, the opposite trend in helping ethene

Please cite this article in press as: Zhang et al., Water-assisted shape-selective production of ethene in methanol-to-olefins reaction on SAPO-34, Chem Catalysis (2024), https://doi.org/10.1016/j.checat.2024.101025

CellPress

production or depressing the formation of other higher olefin products (such as propene and butene) and the improvement in the selectivity of light olefins ($C_2^=$-$C_4^=$) indicates that the presence of water not only inhibits the hydrogen transfer reactions[50] but also may improve ethene generation in an as-yet uncertain manner. It is worth noting that, while increasing the water content can enhance ethene selectivity to some extent, unlimitedly increasing the water levels should be avoided. Too much water cofeeding would cause a decrease in the methanol conversion rate and catalyst structural damage, which are detrimental to improving the yield of olefin products.

Retained organics and coke in SAPO-34

Mechanistically, the conversion of methanol into light olefins follows HCP mechanisms, including multiple catalytic cycles, such as the alkene-based cycle, aromatic-based cycle, and cyclopentadiene-base cycle,[35–37] involving successive methylation of active HCP intermediate species of alkenes, aromatics, or cyclopentadienes, and follows elimination of olefin products. The preferred catalytic reaction cycles for alkene generation are closely related to the acidity and structure of the zeolite catalysts, the generated HCP intermediates in the zeolite, and the reaction conditions, which lead to differences in the product formation and distribution. For instance, ethene was usually produced from the aromatic-based cycle via a polymethylbenzene-induced HCP route, while propene and other higher alkenes usually can be generated via an alkene-based cycle with olefin intermediates.[36,37] Therefore, to further reveal the effect of water on the olefin production, the retained species in methanol-reacted SAPO-34 were investigated and analyzed during the water-cofeeding MTO reaction with varying water contents. As shown in Figure 2A, analyzed and identified by GC-MS, the main retained species (CCl_4-soluble fractions, named "soluble coke") on SAPO-34 were mainly composed of methylbenzenes, naphthalene, methylnaphthalenes, phenanthrene, and pyrene after methanol conversion (time on stream [TOS] = 48 min, methanol conversion 100%), and there were no significant differences in the retained compounds with the increase in cofeeding water content from 1:0 to 1:6 (methanol/water [molar ratio]). However, the amount of coke deposition decreased from 9.0 to 7.9 wt % with increasing cofeeding water (Figure 2B), implying that the addition of water in the MTO reaction system resulted in a significant decrease in coke deposition rate (0.202–0.179 mg min^{-1}, Table S2). More importantly, with increasing cofeeding water, in addition to the depression of coke deposition, the soluble coke became more dominant among the coke species, and the fraction of insoluble coke (the residual heavier counterparts) was reduced (Figure 2B). This suggests that water cofeeding can reduce coke deposition and suppress the transformation of soluble coke to insoluble coke and, thus, improves the catalyst's lifetime. On fully deactivated SAPO-34, the coke content increased from 12.3 to 14.0 wt % (Figure S4) with water content increase from 1:0 to 1:6 (methanol/water [molar ratio]). At this moment, the retained species without or with water cofeeding mainly consisted of methylbenzenes, naphthyl species, phenanthrene, and pyrene. Our previous works indicated that cofed water helped to promote methanol conversion by extending the reaction zone of the SAPO-34 crystal to accommodate more coke deposition, thus contributing to a more efficient catalyst utilization in a long reaction duration.[22,41]

Soluble coke species are mainly composed of methylbenzenes, naphthyl species, phenanthrene, and pyrene, among which methylbenzenes and naphthyl species can behave as reactive HCP species to catalyze the MTO reaction over SAPO-34. The distribution of aromatic species among coke over SAPO-34 was analyzed and is shown in detail in Figure 2C. With the cofed water ratio increased from 1:0 to

Please cite this article in press as: Zhang et al., Water-assisted shape-selective production of ethene in methanol-to-olefins reaction on SAPO-34, Chem Catalysis (2024), https://doi.org/10.1016/j.checat.2024.101025

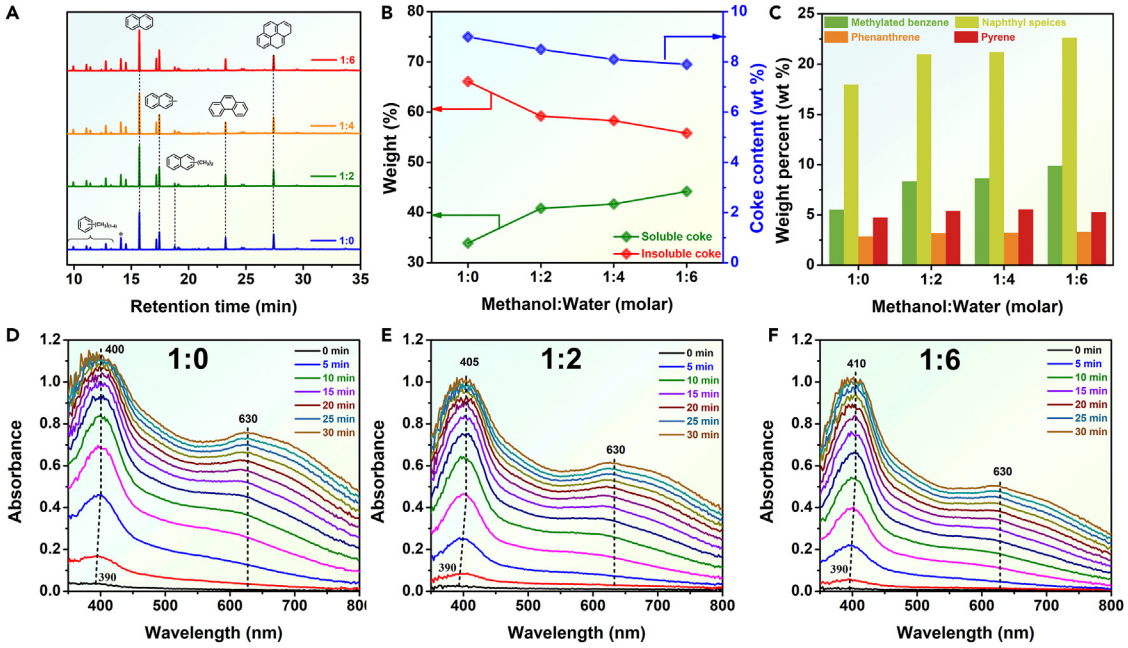

Figure 2. The effects of water on the retained species trapped in SAPO-34 with different water contents

(A) Chromatograms of CCl_4-soluble fractions of the retained organics extracted from the catalyst after methanol conversion.

(B) Total coke content determined by thermogravimetric analysis (TGA) and the fraction of soluble coke and insoluble coke.

(C) Detailed distribution of retained organic species in total coke.

(D–F) UV-vis spectra of SAPO-34 with time on stream during the MTO reaction with different methanol/water ratios.

1:6 (methanol/water [molar ratio]), the proportions of methylbenzene and naphthyl species among total coke obviously increased from 5.5 and 17.8 to 9.9 and 22.6 wt %, respectively, but the proportions of phenanthrene and pyrene remained unchanged. Naphthyl aromatics were predominant among the coke species, and the reactivity of naphthyl species in the MTO reaction on SAPO-34 depends primarily on the reaction temperature. At high temperature, naphthalene and methylnaphthalenes can act as the active HCP species to catalyze the conversion of methanol,[51–53] while at low temperature, they often play the role of inert species that depress the reaction or work as the precursors to form heavy coke.[54,55] Therefore, cofeeding water at low temperatures does not significantly affect ethene selectivity (Figure 1B), while the increase in ethene selectivity at high temperatures may originate from the large amount of naphthyl species working as cocatalysts in SAPO-34 under the water cofeeding reaction condition.

This speculation was further supported and validated by spectroscopic evidence. We performed *in situ* UV-vis spectroscopic experiments to continuously monitor the MTO reaction for 0–30 min on SAPO-34 at 723 K. Under different methanol/water ratios, the MTO reaction on SAPO-34 mainly exhibited absorbance bands at 390–410 and 620–650 nm. The absorption peak at 390–400 nm is usually attributed to the formation of highly methylated phenyl carbocations,[51,52,56–58] which are highly active HCP intermediates. The absorption peak at 400–410 nm is assigned to naphthyl carbocation species, which behave diversely in the MTO process according to the reaction temperature, acting as active HCP species at high temperature or as coke species or coke precursors at low temperature.[51,52] The broad absorption peak observed at 620–650 nm is typically associated with more condensed carbonaceous species derived from PAHs, such as phenanthrene and pyrene.[51,52,56,57] In the

Please cite this article in press as: Zhang et al., Water-assisted shape-selective production of ethene in methanol-to-olefins reaction on SAPO-34, Chem Catalysis (2024), https://doi.org/10.1016/j.checat.2024.101025

CellPress

pure-methanol-fed reaction (Figure 2D), the absorption band at 390 nm, associating with the formation of highly methylated benzene carbocations, was intensified quickly during the initial MTO reaction stage. With the proceeding of the MTO reaction, the absorbance at 390 nm gradually shifted to 400 nm, which can be attributed to the formation of naphthyl carbocations. Simultaneously, the absorbance at ~630 nm from the polycyclic aromatic species exhibited a high intensity, suggesting that the phenyl and naphthyl species were quickly transformed into polycyclic aromatics during the pure methanol feed. However, the addition of water to the MTO reaction resulted in a decrease in the absorbance at both 400 and 630 nm (Figures 2E and 2F), and the pronounced weakening trend at 630 nm indicates that cofeeding water could efficiently inhibit the transformation of methylated benzene and naphthyl species into more heavily condensed aromatic species and thus reduce the rate of coke formation and delay the catalyst deactivation. More interestingly, compared to the pure methanol feed, the absorption band at 400 nm gradually shifted toward 405 nm at a methanol/water ratio of 1:2 and toward 410 nm at a ratio of 1:6. These *in situ* observations further suggest that the addition of water not only inhibits the formation of PAHs but also enhances the proportion of naphthyl species in the retained species, which should be a key factor in the significantly enhanced ethene selectivity in the MTO reaction on SAPO-34 at high reaction temperature under the cofeeding water conditions. Furthermore, for the reaction conducted at a low temperature of 623 K (Figure S5), the addition of water resulted in a reduction in the intensity of the absorption bands at 390–400 and 630 nm, but almost no observable signal shift of the absorption band at ~390 nm was detected. These results indicate that addition of water can inhibit all the confined aromatic formation to some extent, and this does not change the predominance of the methylated benzene species as the main HCP intermediates at low temperature. These observations correspond to the very close catalytic performances of the varied water cofeeding reactions as shown in Figures 1A and 1B.

Naphthyl-based cycle promoting ethene selectivity with the participation of water

To reveal the impact of cofeeding water on the MTO reaction pathway, we conducted $^{12}C/^{13}C$-CH_3OH isotope switching experiments after ^{12}C-CH_3OH reaction at 773 K for 30 min to trace the distribution of C atoms from ^{13}C-CH_3OH among the olefin products and retained organic species under reaction conditions without (methanol/water = 1:0) or with water cofeeding (methanol/water = 1:4). As shown in Figure 3, after the ^{13}C-CH_3OH was fed for 15, 30, and 45 s, both the effluents and the trapped organic species on SAPO-34 exhibited ^{13}C atom incorporation due to the interaction between ^{13}C-CH_3OH and the previously formed ^{12}C-reactive intermediates, from which olefins can be generated. As the reaction was performed at high temperature, the high conversion rate caused more than 80% ^{13}C incorporation in all effluents, and the ^{13}C incorporation was enhanced with prolonging the ^{13}C-CH_3OH feeding time to 15–45 s, as shown in Figure 3A. Surprisingly, compared to feeding methanol alone, increased ^{13}C incorporation in ethene and decreased ^{13}C incorporation in C_3-C_5 alkenes with cofeeding water were observed. This suggests that the impact of water on the formation of ethene and other higher olefins is different. The ^{13}C incorporation of retained aromatic species on SAPO-34 was also analyzed and is shown in Figures 3B and 3C. Compared to the methanol feeding alone, all retained aromatic species, including toluene, xylene, trimethylbenzene (tri-MB), tetramethylbenzene (tetra-MB), naphthalene, methylnaphthalene (MN), and dimethylnaphthalene (DiMN) species, showed a higher ^{13}C incorporation with the assistance of water, confirming that the benzyl and naphthyl species were promoted as more reactive HCP species for methanol conversion on SAPO-34. In addition, only trace amounts of

Please cite this article in press as: Zhang et al., Water-assisted shape-selective production of ethene in methanol-to-olefins reaction on SAPO-34, Chem Catalysis (2024), https://doi.org/10.1016/j.checat.2024.101025

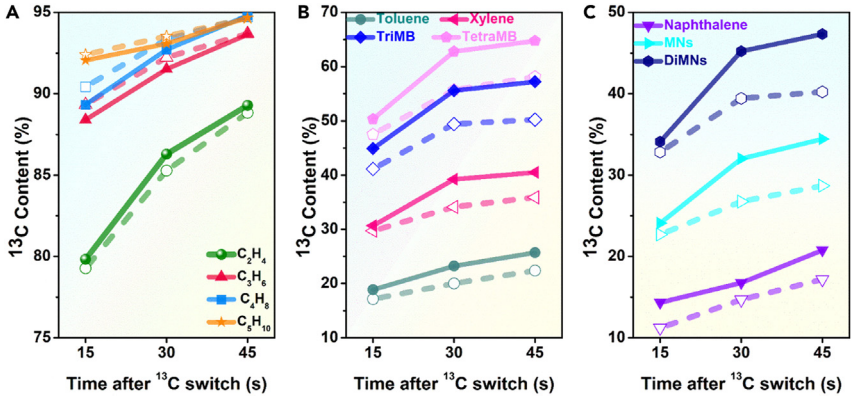

Figure 3. Relative ^{13}C content of the effluent products and the trapped aromatics on SAPO-34 zeolite after ^{12}C-methanol reaction at 773 K for 30 min and switch to ^{13}C-methanol reaction without water cofeeding (dotted line) and with water cofeeding (solid line)

(A) Relative ^{13}C content of effluent products.

(B) Relative ^{13}C content of trapped benzyl species.

(C) Relative ^{13}C content of trapped naphthyl species.

pentamethylbenzene (penta-MB) and hexamethylbenzene (hexa-MB) could be captured in the MTO reaction at high temperature in this work, so their ^{13}C incorporation was not given due to the inaccurate evaluation.

The higher ^{13}C content of ethene compared with that of C_3-C_5 alkenes (Figure 3A) suggests that the ethene and other C_3+ alkenes were generated via different routes. In addition, the ^{13}C content of alkene products was always higher than that of active aromatics (methylbenzyl and naphthyl species) in the CHA cavities of SAPO-34. These observations indicate that the production of alkenes should be generated via alkene-based and aromatic-based cycles at the high reaction temperature regardless of whether or not water was cofed. More specifically, ethene should be generated via alkene-based and aromatic-based cycles, while the other higher alkenes were mainly produced via the alkene-based cycle; otherwise, the higher alkenes should exhibit the same trend of ^{13}C incorporation as ethene. The parallel propagation of alkene-based and aromatic-based cycles would produce more alkene intermediates, which would promote the alkene-based cycle to some extent via methylation and cracking. Indeed, the high temperature would facilitate the cracking of higher alkenes to form ethene, as demonstrated by experimental and theoretical studies.[59,60] However, note that cofeeding water depresses the occurrence of the MTO reaction via the route of the alkene-based catalytic cycle, which is evidenced by the lowered ^{13}C atom incorporation in propene, butene, and pentene. Therefore, the promotion of ethene selectivity after water cofeeding should not be attributed to the alkene-based cycle. In fact, the aromatic-based cycle is preferred for methanol conversion on SAPO-34 due to the spatial confinement of long-chain alkene and aromatic HCP intermediates in SAPO-34 with eight-membered ring and CHA cavities.[61,62] The enhancement of ethene selectivity might be closely related to the route via the aromatic-based cycle. As demonstrated by the higher ^{13}C atom incorporation in ethene and the retained active aromatics (methylbenzyl and naphthyl species) (Figure 3), the aromatic-based catalytic cycle for ethene generation was promoted by water. Although these aromatics can also promote ethene formation, the high ethene selectivity might be attributed to the naphthyl species due to the large amount of retained naphthyl derivatives and high reaction temperature in this study. In fact, the role of naphthyl species in promoting

Please cite this article in press as: Zhang et al., Water-assisted shape-selective production of ethene in methanol-to-olefins reaction on SAPO-34, Chem Catalysis (2024), https://doi.org/10.1016/j.checat.2024.101025

ethene formation has been elucidated, showing a high ethene production of ~51%.[49] The naphthyl species play an important role in ethene production. Especially, the isotope tracing revealed that cofeeding water significantly promoted the catalytic reactivity of naphthyl species, as shown in Figure 3C, in which ^{13}C incorporation is largely improved in naphthalene, MN, and DiMN species with water cofeeding, predicting that water will promote the catalytic conversion of methanol via these naphthyl species as the active intermediates. Together, considering the large amount of retained naphthyl derivatives, naphthyl species may behave as more important HCP species that help the efficient methanol conversion. Therefore, it can be inferred that the introduction of water in the MTO reaction on SAPO-34 at high temperature promotes the catalytic cycle based on aromatics, especially the naphthyl-based cycle, and enhances the MTO reaction, causing the predominant production of ethene. The significant increase in ethene selectivity may be attributed to water cofeeding helping the predominance of naphthyl-based species among confined organics in zeolite (Figure 2C), as well as water promoting the generation of ethene via the naphthyl-based HCP catalytic cycle.

Based on the aforementioned results, the cofeeding water in the MTO reaction on SAPO-34 not only increases the proportion of naphthyl species from 17.8 to 22.6 wt % (Figure 2C) but also promotes the reactivity of naphthyl species toward methanol conversion (Figure 3C). To further reveal and confirm the role of water in the catalytic cycle with naphthyl species as intermediates, DFT calculations were employed to evaluate the contribution of water from an energetic perspective. Due to the high reactivity of DiMN in naphthyl species as indicated by the highest ^{13}C incorporation, the Gibbs free energies of the naphthyl-based cycle with DiMN as a critical HCP species were evaluated. According to a previous report,[63,64] in the process of generating DiMN via continuous methylation of naphthalene with methanol, 1,4-dimethylnaphthalene (1,4-DiMN) was favored to be generated and further methylated with methanol. Therefore, the 1,4-DiMN acted as the critical reactive species in the whole naphthyl-based catalytic cycle in this work. A microenvironment MTO reaction over SAPO-34 with 1,4-DiMN accommodation in the CHA cavities was applied in the adsorption and reaction of the 1,4-DiMN-based catalytic cycle, in which the water molecules were adsorbed around the BAS and then they transformed into a protonated water cluster confined in the 8-MR pore opening (Figure S7). The adsorption enthalpies and Gibbs free energies of 1,4-DiMN confined within the CHA cage with/without water at 773 K were calculated to compare their steric stability (Table S3), and the relatively low adsorption enthalpies and Gibbs free energies with water assistance suggest that water molecules can promote the accommodation of 1,4-DiMN in the CHA cavity. The full catalytic cycle for ethene and propene formation with 1,4-DiMN and the Gibbs free energy barriers and reaction rate constants of methanol conversion are shown in Figure 4 and Table 1, respectively.

For the generation of ethene, 1,4-DiMN proceeds with an ipso methylation (IM1) at the α-C atom with methanol to form the gem-methylated 1,1,4-trimethyl naphthyl cation (TMN^+). This methylation step is known to be a crucial step for triggering the catalytic cycle.[63,64] Subsequently, the TMN^+ is deprotonated (DP1) in the para position of the gem-methyl group to form the exocyclic double bond. This exocyclic double bond further undergoes methylation (M2) to generate the ethene precursor, 1,1-dimethyl-4-ethyl naphthyl cation ($DMEN^+$). Then the gem-methyl group at the α-C atom migrates to the para position by three steps of methyl shifts (TM1/2/3). Finally, ethene is produced via a concerted mechanism with the breaking of the C–C bond and the deprotonation of the terminal methyl group of the ethyl side chain simultaneously. With ethene elimination, the initial 1,4-DiMN is regenerated,

Please cite this article in press as: Zhang et al., Water-assisted shape-selective production of ethene in methanol-to-olefins reaction on SAPO-34, Chem Catalysis (2024), https://doi.org/10.1016/j.checat.2024.101025

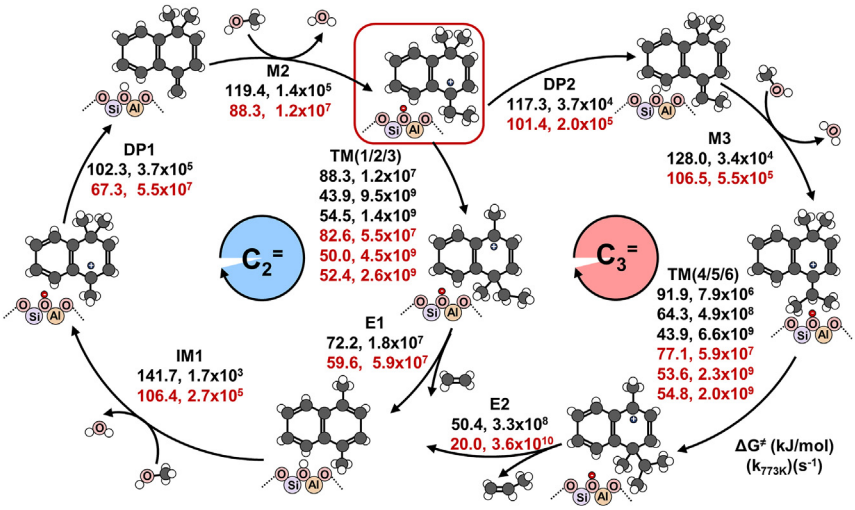

Figure 4. The catalytic cycle for ethene and propene formation

Catalytic cycle of methanol conversion for ethene and propene formation based on the 1,4-DiMN species over SAPO-34 by DFT simulations. The Gibbs free energy and reaction rate constant in the absence of water (black font) and the presence of water (red font) at 773 K are shown.

accomplishing the catalytic cycle. The route of propene formation is similar to the ethene formation in the initial steps. In particular, the $DMEN^+$ undergoes a second exocyclic deprotonation (DP2) and further methylation (M3) to form the 1,1-dimethyl-4-propenyl naphthyl cation ($DMPN^+$). After three methyl shifts (TM4/5/6), propene is generated by the elimination of the isopropyl group (E2), which is similar to ethene formation. For the ethene and propene formation, the free energy barriers of the whole reaction cycle are in the range of 43.9–141.7 kJ/mol in the absence of water (Table 1), illustrating that the catalytic cycle with the 1,4-DiMN species is energetically feasible. The detailed TS structures of all the elementary reactions are shown in Figures S8 and S9.

Water participation in the reaction cycle conducted in the naphthyl-accommodated microenvironment of SAPO-34 gives rise to a remarkable decrease in the free energy barriers of methylation, deprotonation, and elimination, as shown in Table 1.Taking IM1 as an example, the methylation of 1,4-DiMN presents the highest free energy barrier in the whole reaction cycle, but it is noted that the water presence effectively promotes the methylation reaction with a free energy barrier decrease from 141.7 to 106.4 kJ/mol and a reaction rate constant increase from 1.7×10^3 to 2.7×10^5 s^{-1}. The formed water cluster can interact with protonated methanol by H-bond interaction, whereas this special microenvironment can activate the protonated methanol molecule. Correspondingly, as can be seen in Figures 5A1 and 5A2, the C–O bond of methanol is elongated from 1.44 to 1.47 Å with water assistance, causing the high reactivity of methanol in the methylation reaction. The pre-activated methanol molecule can also be reflected by the electrophilicity reactivity of protonated methanol in the methylation reaction. The methylation of 1,4-DiMN with methanol is a typical S_N2 substitution reaction. The f_w^+ of the methyl C atom of methanol was used to evaluate the ability of the nucleophilicity substitution reaction. Compared to the absence of water, the f_w^+ of methanol shows a higher value in the presence of water (Table S4), indicating that such pre-activated methanol molecule tends easily to perform a nucleophilicity substitution reaction with decreased free energy barrier. In addition, the catalytic microenvironment with water assistance can stabilize the TSs of the methylation reaction, leading to the reduction in free energy

Please cite this article in press as: Zhang et al., Water-assisted shape-selective production of ethene in methanol-to-olefins reaction on SAPO-34, Chem Catalysis (2024), https://doi.org/10.1016/j.checat.2024.101025

Table 1. Comparison of the calculated free energy barriers ($\Delta G^{\neq}$) and reaction rate constants (k) for olefin formation via the reaction cycle based on 1,4-DiMN species in the MTO reaction over SAPO-34 at 773 K without/with the assistance of water

	Without water		With water	
Reaction step	$\Delta G^{\neq}$ (kJ/mol)	k (s^{-1})	$\Delta G^{\neq}$ (kJ/mol)	k (s^{-1})
IM1	141.7	1.7×10^{3}	106.4	2.7×10^{5}
DP1	102.3	3.7×10^{5}	67.3	5.5×10^{7}
M2	119.4	1.4×10^{5}	88.3	1.2×10^{7}
TM1	88.3	1.2×10^{7}	82.6	5.5×10^{7}
TM2	43.9	9.5×10^{9}	50.0	4.5×10^{9}
TM3	54.5	1.4×10^{9}	52.4	2.6×10^{9}
E1	72.2	1.8×10^{7}	59.6	5.9×10^{7}
DP2	117.3	3.7×10^{4}	101.4	2.0×10^{5}
M3	128.0	3.4×10^{4}	106.5	5.5×10^{5}
TM4	91.9	7.9×10^{6}	77.1	5.9×10^{7}
TM5	64.3	4.9×10^{8}	53.6	2.3×10^{9}
TM6	43.9	6.6×10^{9}	54.8	2.0×10^{9}
E2	50.4	3.3×10^{8}	20.0	3.6×10^{10}

barrier. As depicted by isosurface plots of the reduced density gradient (RDG) in Figure 5, compared to the isosurface of the TS species for IM1 in the absence of water (Figure 5E1), the isosurface of the TS species for IM1 with water assistance (Figure 5E2) exhibits a large green region around the 8-MR pore, which originates from the interaction between the zeolite framework and the organic species together with the water cluster. Consistent with the IM1, the M2 and M3 also present a lower energy barrier with water assistance (Table 1). Apart from the methylation, attention should be warranted on the steps of deprotonation and olefin elimination. It has been reported that water can act as a bridge in the form of a hydrogen acceptor to transport protons bilaterally between the organic species and the acid sites of zeolite.[42–47] Taking the deprotonation reaction (DP1) as an example, the crucial difference in the absence or presence of water is reflected by the recovery of the protonated H^+ in the organic species to conjugate the base oxygen atom of the framework (zeo-) or the O atom of water. Without water assistance, TMN^+ loses its proton of the methyl side chain to the framework O atom directly (Figure 5B1), showing a reaction free barrier energy of 102.3 kJ/mol. However, with water assistance, this proton preferentially migrates to the O atom of water (as proton acceptor), and subsequently the proton transfers to the framework (Figure 5B2), which significantly facilitates the deprotonation with a lower reaction energy barrier of 67.3 kJ/mol. The elimination of ethene (E1) is also promoted by water with a free energy barrier decrease from 72.2 to 59.6 kJ/mol, thereby acting as a bridge between the organic species and the acid site of zeolite (Figures 5C1 and 5C2). Similar promotions with water participation were also found in the steps DP2 and E2 for propene formation. For the other elementary steps (TM1–6) in the catalytic cycle, a slight influence of the free energy barrier of 2–14 kJ/mol induced by the water-mediated environment can be observed. These results elucidate the feasibility of a catalytic cycle with 1,4-DiMN species on SAPO-34 and demonstrate that cofeeding water effectively promotes this catalytic cycle to produce alkenes with lower energy barriers.

The bifurcation for producing ethene and propene was indicated with a red box in Figure 4, which would determine the priority routes for ethene or propene formation. When the $DMEN^+$ forms, it can not only act as the precursor for ethene formation, but also undergo the deprotonation reaction. In this parallel reaction

Please cite this article in press as: Zhang et al., Water-assisted shape-selective production of ethene in methanol-to-olefins reaction on SAPO-34, Chem Catalysis (2024), https://doi.org/10.1016/j.checat.2024.101025

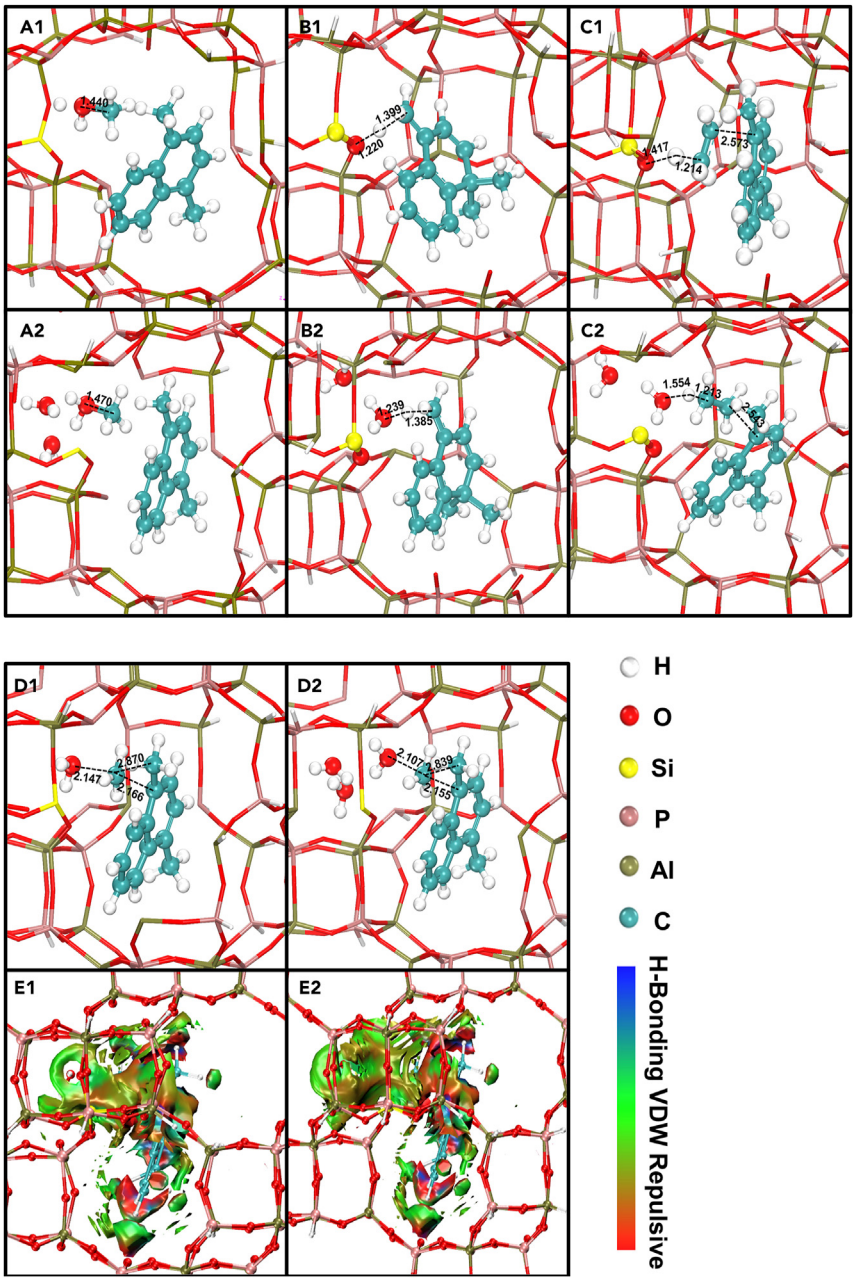

Figure 5. DFT simulation results of the ethene and propene formation based on the 1,4-DiMN species over SAPO-34

(A) Optimized structures for the reactant of IM1 (A1, A2 [assistance of water]).
(B) The transition state of the deprotonation (DP1) (B1, B2 [assistance of water]).
(C) The transition state of the ethene elimination (E1) (C1, C2 [assistance of water]).
(D) The transition state of the methylation of 1,4-DiMN (IM1) (D1, D2 [assistance of water]).
(E) Isosurface plots of the RDG for IM1 (E1, E2 [assistance of water]).

step of $DMEN^+$ conversion, the free energy barrier for methyl shifts (TM1/2/3) to 50.0–82.6 kJ/mol lower than the DP2 of 101.4 kJ/mol along with a higher reaction rate constant by two orders of magnitude in the presence of water. This result suggests that $DMEN^+$ tends to follow the catalytic cycle of ethene formation rather than that of propene, which may lead to the favorable formation of ethene over

Please cite this article in press as: Zhang et al., Water-assisted shape-selective production of ethene in methanol-to-olefins reaction on SAPO-34, Chem Catalysis (2024), https://doi.org/10.1016/j.checat.2024.101025

that of propene. To get further insight into the preferential alkene product, the Gibbs free energy barriers for generating the precursors of ethene and propene, the naphthyl cation with ethyl (M2, $DMEN^+$) or propyl (M3, $DMPN^+$) side chain, and their stabilities in the presence of water were compared. The generation of ethene precursor (M2) needs to overcome the free energy barrier of 88.3 kJ/mol, which is lower by 18.2 kJ/mol than the value of propene precursor formation (M3, 106.5 kJ/mol). Despite the fact that water can promote the M2 and M3 reaction with a lower free energy barrier, the water presents an obvious promotion effect on M2. Remarkably, the free energy barrier of M3 decreased by 21.6 kJ/mol; nevertheless, the free energy barrier of M2 decreased by 31.1 kJ/mol, which indicates that the ethene precursor is more effectively promoted by water than the propene precursor and thus further promotes the formation of ethene. In addition, alkene precursor formation might also be related to the steric constraint of the SAPO-34 microenvironment. This cavity microenvironment energetically favors the stabilization of small-sized $DMEN^+$ (ΔG_{ads} −131.3 kJ/mol) over that of bulky sized $DMPN^+$ (ΔG_{ads} −89.1 kJ/mol) with the presence of water (the adsorption enthalpies and adsorption free energies are listed in Table S5). The competitive reaction steps (DP2 vs. TM1–3), the formation of alkene precursors, and their stabilization together demonstrated the role of water in promoting ethene formation, which is well consistent with higher ethene selectivity presented in our experimental results above (Figure 1D). Except for 1,4-DiMN, naphthalene, with higher content in the CHA cavity (Figure 2A), may also play an important role in producing ethene, so the catalytic cycle based on naphthalene was also calculated to further evaluate the feasibility of the naphthyl-based cycle and the role of water in promoting the naphthyl-based cycle. The catalytic cycle that starts from the methylation of naphthalene with the absence/presence of water is shown in Figure S10. The ethene and propene can be obtained via a series of methylation, deprotonation, and elimination steps, and the detailed TS structures of all the elementary reactions are shown in Figures S11 and S12. Consistent with the result of the 1,4-DiMN-based cycle, the catalytic cycle with naphthalene tends to produce ethene more than propene. Meanwhile, the elementary steps of methylation, deprotonation, and elimination in the catalytic cycle with naphthalene were also facilitated by water molecules (Figure S13), in which the free energy barriers were significantly decreased with water assistance (Table S6). These results evidently demonstrated that the naphthyl species can act as the intermediates for methanol conversion and confirmed the role of water in promoting the catalytic cycle with naphthyl species.

Combining the $^{12}C/^{13}C$-CH_3OH isotope switching experiments and DFT calculations, the preferred reaction pathways to ethylene via the naphthyl-based cycle at high temperature, and the reaction mechanism of water-assisted promotion of naphthyl-based cycle, thus resulting in the improvement of ethene selectivity, has been well demonstrated. Although naphthyl species also formed on SAPO-34 during the MTO reaction at low temperature, the naphthyl-based cycle could not be improved by cofeeding water at low temperature due to the inert role of naphthyl species at low temperature, which usually behaved as the coke species or the precursor to heavy coke instead of HCP intermediates,[54,55] and eventually no obvious changes were presented in ethene selectivity or E/P ratio (Figure 1B) at low temperature in the MTO reaction. Comparatively, the initiation and function of the naphthalene cycle at high temperature and the help of water make ethene the dominant reaction product of the MTO reaction, reflecting variable reaction pathways and product selectivity, indicating the potential for and possibility of regulating olefin products in the MTO process.

Please cite this article in press as: Zhang et al., Water-assisted shape-selective production of ethene in methanol-to-olefins reaction on SAPO-34, Chem Catalysis (2024), https://doi.org/10.1016/j.checat.2024.101025

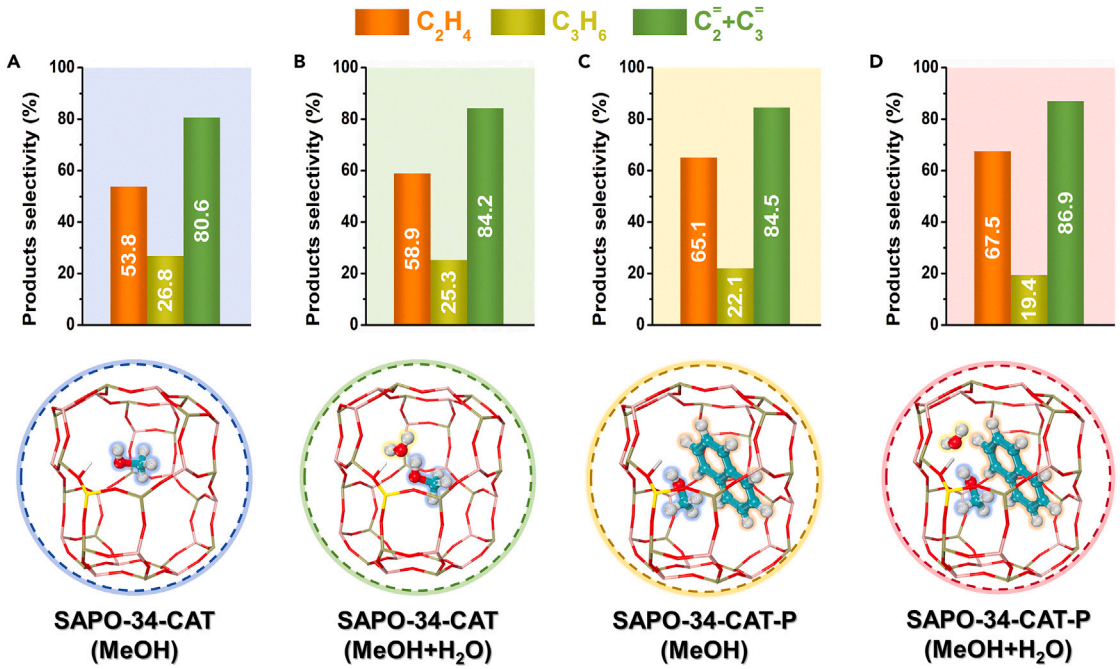

Figure 6. The product selectivity over different catalysts in the MTO reaction with a WHSV of 2 h^{-1} at 773 K

(A) Product selectivity over SAPO-34-CAT without water.

(B) Product selectivity over SAPO-34-CAT with water assistance.

(C) Product selectivity over SAPO-34-CAT-P without water.

(D) Product selectivity over SAPO-34-CAT-P with water assistance.

The strategy for improving ethene selectivity in the MTO reaction on SAPO-34-CAT

The achievement of the production of a specifically required olefin in the MTO reaction is a long-term goal in both academia and industry. Based on the above knowledge that water cofeeding favors the naphthyl-based cycle and promotes the formation of ethene, we prepared pre-coked SAPO-34-CAT (SAPO-34-CAT-P) by "pre-coking" treatment on the MTO catalyst (SAPO-34-CAT), and we propose a strategy for improving ethene selectivity by cofeeding water with methanol over this catalyst with naphthyl-species accommodation. As identified by GC-MS and shown in Figure S14, naphthalene and derivatives were the dominant aromatic species confined in the SAPO-34-CAT-P. The product selectivity on methanol conversion in the absence/presence (methanol/water [molar ratio] = 1:6) of water cofeeding was compared and is shown in Figures 6 and S15, showing that the C_2-C_3 olefin selectivity over the SAPO-34-CAT and SAPO-34-CAT-P was promoted by water cofeeding. In the initial period of the MTO reaction (Figure S15, TOS = 3 min), the ethene selectivity over SAPO-34-CAT presented a relatively low value of 29.2% and further slightly increased to 32.2% with cofed water. However, with the progress of reaction and accumulation of HCPs (especially naphthyl species), the ethene selectivity showed a high value of 53.8%, and it was significantly promoted to 58.9% by water assistance (TOS = 63 min, Figures 6A and 6B), which indicated the role of water and naphthyl species in facilitating ethene formation. More importantly, the SAPO-34-CAT-P, accommodating abundant naphthyl species, showed a high value of ethene selectivity of 65.1% in the high-efficiency reaction period (TOS = 33 min, Figure 6C) in the absence of water. Furthermore, the ethene selectivity can be boosted to 67.5% with the assistance of water (Figure 6D), which

Please cite this article in press as: Zhang et al., Water-assisted shape-selective production of ethene in methanol-to-olefins reaction on SAPO-34, Chem Catalysis (2024), https://doi.org/10.1016/j.checat.2024.101025

increased by 13.7% compared to the SAPO-34-CAT without water cofeeding. These results are well consistent with our experimental work and calculations prediction and evidently confirm the role of water in enhancing the production of ethene by promoting the naphthyl-based cycle. In addition, owing to the more efficient catalyst utilization with the assistance of water, the extension of the catalyst's lifetime can be observed with the water content increased from 1:0 to 1:6 over the SAPO-34-CAT and SAPO-34-CAT-P (Figure S16). Therefore, cofeeding water with methanol over pre-coking SAPO-34-CAT would be an applicable route to greatly improve ethene production in the MTO industry.

Conclusion

In summary, this work reports a remarkable ethene selectivity of 57.7% and an extension of catalyst lifespan with water cofeeding during the MTO reaction at 773 K over SAPO-34, and a joint strategy of cofeeding water with methanol over the naphthyl-species pre-accommodated SAPO-34-CAT-P to obtain high ethene selectivity was proposed. With the aid of GC-MS, *in situ* UV-vis spectroscopy, $^{12}C/^{13}C$-CH_3OH switch experiments, and DFT calculations, the mechanistic role of water in promoting ethene formation and extension of catalyst lifetime was revealed. With water assistance, the catalytic activity toward methanol conversion was promoted and the naphthyl species were preferentially retained in the CHA cages of SAPO-34, resulting in an ethene selectivity increase during MTO reaction at high reaction temperature. DFT calculations revealed that the water-mediated microenvironment can activate the methanol molecule in methanol conversion and simultaneously serve as a proton transfer reagent between the zeolite framework and the organic intermediates. These special water effects contribute to a significant reduction in the reaction free energy barrier for the formation of ethene via the naphthyl-based cycle. Furthermore, the assistance of water can reduce the rate of coke deposition and increase the crystal utilization efficiency of the SAPO-34 zeolite crystal, thereby prolonging the catalyst's lifetime and improving the methanol conversion performance. Inspired by this knowledge, a combined strategy involving the pre-location of naphthyl species into the SAPO-34-CAT and cofeeding water was implemented, leading to a further increase in ethene selectivity to 67.5%. These studies enrich our understanding of the catalytic regulation mechanism of water in the MTO reaction and provide potential solutions for the production of specially desired olefin products via zeolite catalysis.

EXPERIMENTAL PROCEDURES

Resource availability

Lead contact

Requests for further information and resources should be directed to and will be fulfilled by the lead contact, Professor Zhongmin Liu (liuzm@dicp.ac.cn).

Materials availability

This study did not generate new unique reagents.

Data and code availability

The published article includes all datasets generated or analyzed during this study.

Catalyst preparation

The SAPO-34 zeolite was synthesized by the traditional hydrothermal method according to our previous work.[65] The fresh H-form SAPO-34 zeolite was obtained by calcining the crystallized product at 873 K in 100 mL min^{-1} airflow for 6 h to remove the organic template (named SAPO-34).

Please cite this article in press as: Zhang et al., Water-assisted shape-selective production of ethene in methanol-to-olefins reaction on SAPO-34, Chem Catalysis (2024), https://doi.org/10.1016/j.checat.2024.101025

Catalyst characterization

The powder XRD pattern of the catalyst was tested with a PANalytical X'Pert PRO X-ray diffractometer with Cu-K α radiation (λ = 0.15418 nm) as the X-ray source, operating at 40 kV and 40 mA from 5° to 50°. The chemical composition of the catalyst was determined on a PhilipsMagix-601 X-ray fluorescence (XRF) spectrometer. The morphology of the catalyst was observed by using an SEM (Hitachi SU 8020) with an accelerating voltage of 15 kV. The surface area and pore volume of the catalyst were obtained from nitrogen adsorption-desorption isotherm performed at 77 K on a Micromeritics ASAP 2020 apparatus. The samples were degassed at 623 K under vacuum for 4 h before the test to remove the adsorbed water. The surface area was estimated from the Brunauer-Emmett-Teller (BET) equation. All the solid-state NMR spectra were recorded on a Bruker Avance III 500 MHz spectrometer equipped with an 11.7 T wide-bore magnet. ^{1}H MAS NMR spectra were recorded by using a one pulse sequence with a $\pi/2$ pulse width of 2.85 μs and 20 s recycle delay at 20 kHz, with the adamantane (1.74 ppm) as the chemical shift reference. ^{29}Si MAS NMR spectra were recorded at a spinning rate of 8 kHz using high-power proton decoupling. A total of 5,655 scans were accumulated, with a $\pi/4$ pulse width of 2.25 μs and 10 s recycle delay. Chemical shifts were referenced to kaolinite (−91.5 ppm).

Catalytic tests

Fixed-bed MTO reactions were performed in a quartz-tube reactor with an inner diameter of 6 mm under atmospheric pressure. Typically, the SAPO-34 was pressed, crushed, and sieved to 40–60 mesh, and then 100 mg of catalyst was loaded into the reactor. Prior to the reaction, the catalyst was activated at 793 K under argon flow for 30 min, and then the temperature was adjusted to the reaction temperature of 773 or 623 K. Methanol and water were fed by passing argon through saturation evaporators kept at 288 K for methanol and 323–350 K for water. The molar ratio of methanol to water was regulated by changing the temperature of the water saturation evaporator and carrier gas flow. Additional argon was used as a compensation gas during the pure methanol feed to make sure that the partial pressure and contact time of methanol were consistent in all the cofeeding water experiments. The pre-coked reactions for preparing the catalyst with naphthyl-species accommodation (named SAPO-34-CAT-P) were carried out in a fluidized bed reactor. The MTO catalyst (SAPO-34-CAT) containing SAPO-34 and binders was first activated at 823 K for 30 min, and then 1-butene was fed into the reactor with a WHSV of 2 h^{-1} at 823 K for 5 min. The effluent products were kept at 473 K to avoid condensation and analyzed by an online gas chromatograph (Agilent 7890 B) with a PoraPLOT Q capillary column (27.5 m × 0.32 m × 20 μm) and a flame ionization detector. The conversion and selectivity of the MTO reaction were calculated on a CH_2 basis. The catalytic lifetime in this work was defined as the duration of methanol conversion >99%.

In situ UV-visible spectroscopy

The UV-vis spectroscopic experiments were performed on the Varian Cary 5000 UV-vis-NIR spectrophotometer. The catalytic reactions were carried out on a diffuse reflectance *in situ* reaction cell and heated by the PIKE controller. Typically, 30 mg of catalyst powder was loaded into the reaction cell, and methanol and water were fed by passing nitrogen through saturation evaporators kept at 293 K. The reaction was conducted with a total flow of 40 mL min^{-1}, and the N_2 flow rate was always set at 1.7 mL min^{-1} for passing through the methanol evaporator. The different ratios of methanol to water were obtained by regulating the N_2 flow rate for passing the water evaporator. The spectra were recorded in absorbance mode and saved every 2.5 min after methanol was introduced into the *in situ* reaction cell. The

Please cite this article in press as: Zhang et al., Water-assisted shape-selective production of ethene in methanol-to-olefins reaction on SAPO-34, Chem Catalysis (2024), https://doi.org/10.1016/j.checat.2024.101025

integration time for each spectrum was 0.2 s, and fresh SAPO-34 was used as the blank reference.

$^{12}C/^{13}C$-methanol switch experiments

The $^{12}C/^{13}C$-methanol switch experiments were also conducted at 773 K over SAPO-34 with a WHSV of 2 h^{-1}. The reactants of ^{12}C-methanol and water were introduced into a quartz fixed-bed reactor by passing nitrogen through the saturation evaporators for 30 min. Then the feeding of ^{12}C-methanol was stopped and ^{13}C-methanol was fed into the reactor for 15, 30, and 45 s. Subsequently, nitrogen was switched into the reactor to purge the catalyst bed and the reactor was immediately quenched by sufficient liquid nitrogen to stop the reaction. The isotopic distribution of gas effluents and the retained organic species confined in the catalyst were analyzed by GC-MS (Agilent 7890B/5977A).

Confined organics determination

The total coke content of spent catalyst was tested by thermogravimetric analysis (TGA) measured on an SDTQ 600 instrument. Typically, about 10 mg of spent catalyst was loaded and heated from room temperature to 1,173 K at a heating rate of 10 K min^{-1} under 100 mL min^{-1} airflow. The total coke content was calculated based on the weight loss at the temperature range of 523–1,173 K. As for coke species, 25.0 mg of spent catalyst was first dissolved in 0.5 mL 20% HF solution in a Teflon vial and extracted with 0.5 mL CCl_4 with C_2Cl_6 as interior label. The CCl_4-extracted organics thereafter were called "soluble coke" and identified by GC-MS equipped with an HP-5 capillary column and a flame ionization detector.

Theoretical calculation method

For theoretical calculations, a 92 T cluster model ($Al_{46}P_{45}SiO_{157}H_{55}$) represented the structure of SAPO-34 zeolite as shown in Figure S6, which was extracted from the crystallographic CHA structure of the International Zeolite Association. For the extended zeolite model, the terminal Al–H and P–H bonds with fixed bond lengths of 1.55 and 1.35 Å, respectively, were oriented along the directions of the corresponding Al–O and P–O bonds. The location of Brønsted acid was chosen at the O (2) site (one 4-MR and two 8-MRs) in the 8-MR pore opening, accessible for adsorbents and surrounded by maximum reaction space.[66]

In this work, the optimization of various adsorption structures and TSs was conducted using the ONIOM (ωB97XD/6-31G(d,p):AM1) method.[67] To preserve original zeolite structure, only terminal hydrogen atoms were fixed at crystallographic locations and other atoms were relaxed. The frequency calculations were performed at the same level as geometry optimizations to ensure that the saddle points exhibited the proper number of imaginary frequencies. The single-point energy was calculated with the ωB97XD/6-31G(d,p) method and corrected by zero-point energy to obtain highly accurate energy. In order to correlate to the real MTO reaction conditions, the adsorption enthalpies or Gibbs free energies (ΔH_{ads} or ΔG_{ads}) of the initial naphthyl-species molecule and intrinsic free energy barriers ($\Delta G^{\neq}$) for key elementary reaction in the reaction routes were obtained from the above total electronic energies and the thermal correction from frequency calculations. The temperature and pressure were 773 K and 1 atm. All DFT calculations were performed using the Gaussian 09 software package.[68] The reaction rate constants were obtained through TS theory (TST) as implemented in the TAMkin program.[69]

The conceptual DFT (CDFT)[70] initially developed by Robert G. Parr aims to unravel favorable reactive sites of chemical systems or reactivity of different chemical

species. Hereinto, the Fukui function (f) and dual descriptor (Δf) are the most robust method for predicting favorable reactive sites in electrophilic/nucleophilic reactions. Like f or Δf, the orbital-weighted Fukui function (f_w) and dual descriptor (Δf_w) are special for systems with degenerate or nearly degenerate frontier molecular orbitals.[71,72] And its condensed version is the integration in Hirshfeld atomic spaces to quantitatively determine the net amount of f_w or Δf_w of every atom. The definitiond of f_w and Δf_w are as follows:

$$f_w^+(r) = \sum_{i=LUMO}^{\infty} w_i|\varphi_i(r)|^2 \; w_i = \frac{exp\left[-\left(\frac{\mu-\varepsilon_i}{\Delta}\right)^2\right]}{\sum_{i=LUMO}^{\infty} exp\left[-\left(\frac{\mu-\varepsilon_i}{\Delta}\right)^2\right]},$$

$$f_w^-(r) = \sum_{i}^{HOMO} w_i|\varphi_i(r)|^2 \; w_i = \frac{exp\left[-\left(\frac{\mu-\varepsilon_i}{\Delta}\right)^2\right]}{\sum_{i}^{\infty HOMO} exp\left[-\left(\frac{\mu-\varepsilon_i}{\Delta}\right)^2\right]},$$

$$\Delta f_w(r) = f_w^+(r) - f_w^-(r).$$

Here, high values of $f_w^+(r)$ or $f_w^-(r)$ indicate the most favorable places to receive or donate electrons characterizing sites of nucleophilic attack or electrophilic attack. The $f_w^+(r)$ and $f_w^-(r)$ were calculated with the Multiwfn software.[73]

The RDG (RDG(r) = $1/(2(3\pi^2)^{(1/3)})|\nabla\rho(r)|/(\rho(r)^{(4/3)})$), together with electron density, was adopted to describe the noncovalent interactions between the adsorbed organic species and the zeolite framework. The sign of the second largest eigenvalue ($\lambda 2$) of the electron density Hessian can be used to distinguish bonded ($\lambda 2 < 0$) from nonbonded ($\lambda 2 > 0$) interactions. Furthermore, the sign of $\lambda 2$ can identify different types of noncovalent interactions: $sign(\lambda 2)\rho < 0$, H-bonding interaction; $sign(\lambda 2)\rho \approx 0$, weak van der Waals (vdW) interaction; and $sign(\lambda 2)\rho > 0$, strong repulsive interaction. The RDG functions and $sign(\lambda 2)\rho$ were calculated with the Multiwfn software.[73]

SUPPLEMENTAL INFORMATION

Supplemental information can be found online at https://doi.org/10.1016/j.checat.2024.101025.

ACKNOWLEDGMENTS

We thank the following funding agencies for supporting this work: the National Natural Science Foundation of China (22372163, 21991092, 21991090, 21902153, 22288101, 22372169), the National Key R&D Program of China (2021YFA1502600), and the Youth Innovation Promotion Association, CAS (2022182).

AUTHOR CONTRIBUTIONS

C.Z. and X.W. conceived the study, coordinated the research, and designed the experiments. Y.Z. and W.Z. conducted the theoretical calculations. S.L. helped in conducting $^{12}C/^{13}C$-methanol switch experiments. C.L. and S.X. performed the MAS NMR experiments. D.H. and L.W. prepared the SAPO-34-CAT-P sample. C.Z., X.W., Y.Z., W.Z., Y.W., and Z.L. contributed to writing and revising the manuscript. Y.W. and Z.L. supervised the scientific work and led the collaborative efforts. All authors discussed the results and commented on the manuscript.

Please cite this article in press as: Zhang et al., Water-assisted shape-selective production of ethene in methanol-to-olefins reaction on SAPO-34, Chem Catalysis (2024), https://doi.org/10.1016/j.checat.2024.101025

CellPress

DECLARATION OF INTERESTS

The authors declare no competing interests.

Received: February 26, 2024
Revised: April 23, 2024
Accepted: May 16, 2024
Published: June 11, 2024

REFERENCES

1. Resasco, D.E., Crossley, S.P., Wang, B., and White, J.L. (2021). Interaction of water with zeolites: a review. Catal. Rev.-Sci. Eng. *63*, 302–362.

2. Tee, S.Y., Win, K.Y., Teo, W.S., Koh, L.D., Liu, S., Teng, C.P., and Han, M.Y. (2017). Recent Progress in Energy-Driven Water Splitting. Adv. Sci. *4*, 1600337.

3. Li, G., Wang, B., and Resasco, D.E. (2019). Water-Mediated Heterogeneously Catalyzed Reactions. ACS Catal. *10*, 1294–1309.

4. Wolf, M., Fischer, N., and Claeys, M. (2020). Water-induced deactivation of cobalt-based Fischer–Tropsch catalysts. Nat. Catal. *3*, 962–965.

5. Fang, W., Wang, C., Liu, Z., Wang, L., Liu, L., Li, H., Xu, S., Zheng, A., Qin, X., Liu, L., and Xiao, F.S. (2022). Physical mixing of a catalyst and a hydrophobic polymer promotes CO hydrogenation through dehydration. Science *377*, 406–410.

6. Liu, Z., Huang, E., Orozco, I., Liao, W., Palomino, R.M., Rui, N., Duchoň, T., Nemšák, S., Grinter, D.C., Mahapatra, M., et al. (2020). Water-promoted interfacial pathways in methane oxidation to methanol on a CeO_2-Cu_2O catalyst. Science *368*, 513–517.

7. Pfriem, N., Hintermeier, P.H., Eckstein, S., Kim, S., Liu, Q., Shi, H., Milakovic, L., Liu, Y., Haller, G.L., Baráth, E., et al. (2021). Role of the ionic environment in enhancing the activity of reacting molecules in zeolite pores. Science *372*, 952–957.

8. Yarulina, I., Chowdhury, A.D., Meirer, F., Weckhuysen, B.M., and Gascon, J. (2018). Recent trends and fundamental insights in the methanol-to-hydrocarbons process. Nat. Catal. *1*, 398–411.

9. Tian, P., Wei, Y., Ye, M., and Liu, Z. (2015). Methanol to Olefins (MTO): From Fundamentals to Commercialization. ACS Catal. *5*, 1922–1938.

10. Olsbye, U., Svelle, S., Lillerud, K.P., Wei, Z.H., Chen, Y.Y., Li, J.F., Wang, J.G., and Fan, W.B. (2015). The formation and degradation of active species during methanol conversion over protonated zeotype catalysts. Chem. Soc. Rev. *44*, 7155–7176.

11. Wang, M., Jaegers, N.R., Lee, M.S., Wan, C., Hu, J.Z., Shi, H., Mei, D., Burton, S.D., Camaioni, D.M., Gutiérrez, O.Y., et al. (2019). Genesis and Stability of Hydronium Ions in Zeolite Channels. J. Am. Chem. Soc. *141*, 3444–3455.

12. Vjunov, A., Wang, M., Govind, N., Huthwelker, T., Shi, H., Mei, D., Fulton, J.L., and Lercher, J.A. (2017). Tracking the Chemical Transformations at the Brønsted Acid Site upon Water-Induced Deprotonation in a Zeolite Pore. Chem. Mater. *29*, 9030–9042.

13. Chen, K., Kelsey, J., White, J.L., Zhang, L., and Resasco, D. (2015). Water Interactions in Zeolite Catalysts and Their Hydrophobically Modified Analogues. ACS Catal. *5*, 7480–7487.

14. Eckstein, S., Hintermeier, P.H., Zhao, R., Baráth, E., Shi, H., Liu, Y., and Lercher, J.A. (2019). Influence of Hydronium Ions in Zeolites on Sorption. Angew. Chem. Int. Ed. *58*, 3450–3455.

15. Sun, T., Xu, S., Xiao, D., Liu, Z., Li, G., Zheng, A., Liu, W., Xu, Z., Cao, Y., Guo, Q., et al. (2020). Water-Induced Structural Dynamic Process in Molecular Sieves under Mild Hydrothermal Conditions: Ship-in-a-Bottle Strategy for Acidity Identification and Catalyst Modification. Angew. Chem. Int. Ed. *59*, 20672–20681.

16. Yang, L., Wang, C., Zhang, L., Dai, W., Chu, Y., Xu, J., Wu, G., Gao, M., Liu, W., Xu, Z., et al. (2021). Stabilizing the framework of SAPO-34 zeolite toward long-term methanol-to-olefins conversion. Nat. Commun. *12*, 4661.

17. De Wispelaere, K., Wondergem, C.S., Ensing, B., Hemelsoet, K., Meijer, E.J., Weckhuysen, B.M., Van Speybroeck, V., and Ruiz-Martínez, J. (2016). Insight into the Effect of Water on the Methanol-to-Olefins Conversion in H-SAPO-34 from Molecular Simulations and in Situ Microspectroscopy. ACS Catal. *6*, 1991–2002.

18. Marchi, A.J., and Froment, G.F. (1991). Catalytic conversion of methanol to light alkenes on SAPO molecular sieves. Appl. Catal. *71*, 139–152.

19. Marchi, A.J., and Froment, G.F. (1993). Catalytic conversion of methanol into light alkenes on mordenite-like zeolites. Appl. Catal. A-Gen. *94*, 91–106.

20. Wu, X., and Anthony, R.G. (2001). Effect of feed composition on methanol conversion to light olefins over SAPO-34. Appl. Catal. A-Gen. *218*, 241–250.

21. Ghavipour, M., Behbahani, R.M., Moradi, G.R., and Soleimanimehr, A. (2013). Methanol dehydration over alkali-modified H-ZSM-5; effect of temperature and water dilution on products distribution. Fuel *113*, 310–317.

22. Zhao, X., Li, J., Tian, P., Wang, L., Li, X., Lin, S., Guo, X., and Liu, Z. (2019). Achieving a Superlong Lifetime in the Zeolite-Catalyzed MTO Reaction under High Pressure: Synergistic Effect of Hydrogen and Water. ACS Catal. *9*, 3017–3025.

23. Shoinkhorova, T., Cordero-Lanzac, T., Ramirez, A., Chung, S.-h., Dokania, A., Ruiz-Martinez, J., and Gascon, J. (2021). Highly Selective and Stable Production of Aromatics via High-Pressure Methanol Conversion. ACS Catal. *11*, 3602–3613.

24. Lin, S., Zhi, Y., Zhang, W., Yuan, X., Zhang, C., Ye, M., Xu, S., Wei, Y., and Liu, Z. (2023). Hydrogen transfer reaction contributes to the dynamic evolution of zeolite-catalyzed methanol and dimethyl ether conversions: Insight into formaldehyde. Chin. J. Catal. *46*, 11–27.

25. Liu, R., Shao, X., Wang, C., Dai, W., and Guan, N. (2023). Reaction mechanism of methanol-to-hydrocarbons conversion: Fundamental and application. Chin. J. Catal. *47*, 67–92.

26. Wang, S., Qin, Z., Dong, M., Wang, J., and Fan, W. (2022). Recent progress on MTO reaction mechanisms and regulation of acid site distribution in the zeolite framework. Chem Catal. *2*, 1657–1685.

27. Olsbye, U., Svelle, S., Bjørgen, M., Beato, P., Janssens, T.V.W., Joensen, F., Bordiga, S., and Lillerud, K.P. (2012). Conversion of methanol to hydrocarbons: how zeolite cavity and pore size controls product selectivity. Angew. Chem. Int. Ed. *51*, 5810–5831.

28. Lin, S., Zhi, Y., Chen, W., Li, H., Zhang, W., Lou, C., Wu, X., Zeng, S., Xu, S., Xiao, J., et al. (2021). Molecular Routes of Dynamic Autocatalysis for Methanol-to-Hydrocarbons Reaction. J. Am. Chem. Soc. *143*, 12038–12052.

29. Sun, T., Chen, W., Xu, S., Zheng, A., Wu, X., Zeng, S., Wang, N., Meng, X., Wei, Y., and Liu, Z. (2021). The first carbon-carbon bond formation mechanism in methanol-to-hydrocarbons process over chabazite zeolite. Chem *7*, 2415–2428.

30. Wu, X., Xu, S., Zhang, W., Huang, J., Li, J., Yu, B., Wei, Y., and Liu, Z. (2017). Direct Mechanism of the First Carbon-Carbon Bond Formation in the Methanol-to-Hydrocarbons Process. Angew. Chem. Int. Ed. *56*, 9039–9043.

31. Liu, Y., Müller, S., Berger, D., Jelic, J., Reuter, K., Tonigold, M., Sanchez-Sanchez, M., and Lercher, J.A. (2016). Formation Mechanism of the First Carbon-Carbon Bond and the First Olefin in the Methanol Conversion into Hydrocarbons. Angew. Chem. Int. Ed. *55*, 5723–5726.

32. Chowdhury, A.D., Houben, K., Whiting, G.T., Mokhtar, M., Asiri, A.M., Al-Thabaiti, S.A., Basahel, S.N., Baldus, M., and Weckhuysen,

Please cite this article in press as: Zhang et al., Water-assisted shape-selective production of ethene in methanol-to-olefins reaction on SAPO-34, Chem Catalysis (2024), https://doi.org/10.1016/j.checat.2024.101025

B.M. (2016). Initial Carbon-Carbon Bond Formation during the Early Stages of the Methanol-to-Olefin Process Proven by Zeolite-Trapped Acetate and Methyl Acetate. Angew. Chem. Int. Ed. *55*, 15840–15845.

33. Wu, X., Chen, W., Xu, S., Lin, S., Sun, T., Zheng, A., Wei, Y., and Liu, Z. (2021). Dynamic Activation of C1 Molecules Evoked by Zeolite Catalysis. ACS Cent. Sci. *7*, 681–687.

34. Wu, X., Xu, S., Wei, Y., Zhang, W., Huang, J., Xu, S., He, Y., Lin, S., Sun, T., and Liu, Z. (2018). Evolution of C–C Bond Formation in the Methanol-to-Olefins Process: From Direct Coupling to Autocatalysis. ACS Catal. *8*, 7356–7361.

35. Zhang, W., Zhi, Y., Huang, J., Wu, X., Zeng, S., Xu, S., Zheng, A., Wei, Y., and Liu, Z. (2019). Methanol to Olefins Reaction Route Based on Methylcyclopentadienes as Critical Intermediates. ACS Catal. *9*, 7373–7379.

36. Bjorgen, M., Svelle, S., Joensen, F., Nerlov, J., Kolboe, S., Bonino, F., Palumbo, L., Bordiga, S., and Olsbye, U. (2007). Conversion of methanol to hydrocarbons over zeolite H-ZSM-5: On the origin of the olefinic species. J. Catal. *249*, 195–207.

37. Svelle, S., Joensen, F., Nerlov, J., Olsbye, U., Lillerud, K.-P., Kolboe, S., and Bjørgen, M. (2006). Conversion of Methanol into Hydrocarbons over Zeolite H-ZSM-5: Ethene Formation Is Mechanistically Separated from the Formation of Higher Alkenes. J. Am. Chem. Soc. *128*, 14770–14771.

38. Wang, N., Zhi, Y., Wei, Y., Zhang, W., Liu, Z., Huang, J., Sun, T., Xu, S., Lin, S., He, Y., et al. (2020). Molecular elucidating of an unusual growth mechanism for polycyclic aromatic hydrocarbons in confined space. Nat. Commun. *11*, 1079.

39. Yu, B., Zhang, W., Wei, Y., Wu, X., Sun, T., Fan, B., Xu, S., and Liu, Z. (2020). Capture and identification of coke precursors to elucidate the deactivation route of the methanol-to-olefin process over H-SAPO-34. Chem. Commun. *56*, 8063–8066.

40. Lin, S., Zhi, Y., Liu, Z., Yuan, J., Liu, W., Zhang, W., Xu, Z., Zheng, A., Wei, Y., and Liu, Z. (2022). Multiscale dynamical cross-talk in zeolite-catalyzed methanol and dimethyl ether conversions. Natl. Sci. Rev. *9*, nwac151.

41. Wang, N., Wang, L., Zhi, Y., Han, J., Zhang, C., Wu, X., Zhang, J., Wang, L., Fan, B., Xu, S., et al. (2023). Coking and decoking chemistry for resource utilization of polycyclic aromatic hydrocarbons (PAHs) and low-carbon process. J. Energy Chem. *76*, 105–116.

42. Wang, C.M., Wang, Y.D., Xie, Z.K., and Liu, Z.P. (2009). Methanol to Olefin Conversion on HSAPO-34 Zeolite from Periodic Density Functional Theory Calculations: A Complete Cycle of Side Chain Hydrocarbon Pool Mechanism. J. Phys. Chem. C *113*, 4584–4591.

43. De Wispelaere, K., Hemelsoet, K., Waroquier, M., and Van Speybroeck, V. (2013). Complete low-barrier side-chain route for olefin formation during methanol conversion in H-SAPO-34. J. Catal. *305*, 76–80.

44. Wang, S., Chen, Y., Wei, Z., Qin, Z., Chen, J., Ma, H., Dong, M., Li, J., Fan, W., and Wang, J. (2014). Theoretical insights into the mechanism of olefin elimination in the methanol-to-olefin process over HZSM-5, HMOR, HBEA, and HMCM-22 zeolites. J. Phys. Chem. A *118*, 8901–8910.

45. Wang, S., Chen, Y., Wei, Z., Qin, Z., Ma, H., Dong, M., Li, J., Fan, W., and Wang, J. (2015). Polymethylbenzene or Alkene Cycle? Theoretical Study on Their Contribution to the Process of Methanol to Olefins over H-ZSM-5 Zeolite. J. Phys. Chem. C *119*, 28482–28498.

46. Wang, S., Wei, Z., Chen, Y., Qin, Z., Ma, H., Dong, M., Fan, W., and Wang, J. (2015). Methanol to Olefins over H-MCM-22 Zeolite: Theoretical Study on the Catalytic Roles of Various Pores. ACS Catal. *5*, 1131–1144.

47. Zhang, W., Chen, J., Xu, S., Chu, Y., Wei, Y., Zhi, Y., Huang, J., Zheng, A., Wu, X., Meng, X., et al. (2018). Methanol to Olefins Reaction over Cavity-type Zeolite: Cavity Controls the Critical Intermediates and Product Selectivity. ACS Catal. *8*, 10950–10963.

48. Wang, C., Yang, L., Gao, M., Shao, X., Dai, W., Wu, G., Guan, N., Xu, Z., Ye, M., and Li, L. (2022). Directional Construction of Active Naphthalenic Species within SAPO-34 Crystals toward More Efficient Methanol-to-Olefin Conversion. J. Am. Chem. Soc. *144*, 21408–21416.

49. Zhou, J., Gao, M., Zhang, J., Liu, W., Zhang, T., Li, H., Xu, Z., Ye, M., and Liu, Z. (2021). Directed transforming of coke to active intermediates in methanol-to-olefins catalyst to boost light olefins selectivity. Nat. Commun. *12*, 17.

50. Wang, H., Hou, Y., Sun, W., Hu, Q., Xiong, H., Wang, T., Yan, B., and Qian, W. (2020). Insight into the Effects of Water on the Ethene to Aromatics Reaction with HZSM-5. ACS Catal. *10*, 5288–5298.

51. Borodina, E., Sharbini Harun Kamaluddin, H., Meirer, F., Mokhtar, M., Asiri, A.M., Al-Thabaiti, S.A., Basahel, S.N., Ruiz-Martinez, J., and Weckhuysen, B.M. (2017). Influence of the Reaction Temperature on the Nature of the Active and Deactivating Species During Methanol-to-Olefins Conversion over H-SAPO-34. ACS Catal. *7*, 5268–5281.

52. Borodina, E., Meirer, F., Lezcano-González, I., Mokhtar, M., Asiri, A.M., Al-Thabaiti, S.A., Basahel, S.N., Ruiz-Martinez, J., and Weckhuysen, B.M. (2015). Influence of the Reaction Temperature on the Nature of the Active and Deactivating Species during Methanol to Olefins Conversion over H-SSZ-13. ACS Catal. *5*, 992–1003.

53. Song, W., Fu, H., and Haw, J.F. (2001). Selective Synthesis of Methylnaphthalenes in HSAPO-34 Cages and Their Function as Reaction Centers in Methanol-to-Olefin Catalysis. J. Phys. Chem. B *105*, 12839–12843.

54. Wei, Y., Yuan, C., Li, J., Xu, S., Zhou, Y., Chen, J., Wang, Q., Xu, L., Qi, Y., Zhang, Q., and Liu, Z. (2012). Coke formation and carbon atom economy of methanol-to-olefins reaction. ChemSusChem *5*, 906–912.

55. Wei, Y., Li, J., Yuan, C., Xu, S., Zhou, Y., Chen, J., Wang, Q., Zhang, Q., and Liu, Z. (2012). Generation of diamondoid hydrocarbons as confined compounds in SAPO-34 catalyst in the conversion of methanol. Chem. Commun. *48*, 3082–3084.

56. Van Speybroeck, V., Hemelsoet, K., De Wispelaere, K., Qian, Q., Van der Mynsbrugge, J., De Sterck, B., Weckhuysen, B.M., and Waroquier, M. (2013). Mechanistic Studies on Chabazite-Type Methanol-to-Olefin Catalysts: Insights from Time-Resolved UV/Vis Microspectroscopy Combined with Theoretical Simulations. ChemCatChem *5*, 173–184.

57. Hemelsoet, K., Qian, Q., De Meyer, T., De Wispelaere, K., De Sterck, B., Weckhuysen, B.M., Waroquier, M., and Van Speybroeck, V. (2013). Identification of intermediates in zeolite-catalyzed reactions by in situ UV/Vis microspectroscopy and a complementary set of molecular simulations. Chem. Eur J. *19*, 16595–16606.

58. Dai, W., Wu, G., Li, L., Guan, N., and Hunger, M. (2013). Mechanisms of the Deactivation of SAPO-34 Materials with Different Crystal Sizes Applied as MTO Catalysts. ACS Catal. *3*, 588–596.

59. Wang, C.-M., Wang, Y.-D., and Xie, Z.-K. (2013). Insights into the reaction mechanism of methanol-to-olefins conversion in HSAPO-34 from first principles: Are olefins themselves the dominating hydrocarbon pool species? J. Catal. *301*, 8–19.

60. Wu, W., Guo, W., Xiao, W., and Luo, M. (2011). Dominant reaction pathway for methanol conversion to propene over high silicon H-ZSM-5. Chem. Eng. Sci. *66*, 4722–4732.

61. Li, J., Wei, Y., Liu, G., Qi, Y., Tian, P., Li, B., He, Y., and Liu, Z. (2011). Comparative study of MTO conversion over SAPO-34, H-ZSM-5 and H-ZSM-22: Correlating catalytic performance and reaction mechanism to zeolite topology. Catal. Today *171*, 221–228.

62. Hereijgers, B.P., Bleken, F., Nilsen, M.H., Svelle, S., Lillerud, K.-P., Bjørgen, M., Weckhuysen, B.M., and Olsbye, U. (2009). Product shape selectivity dominates the Methanol-to-Olefins (MTO) reaction over H-SAPO-34 catalysts. J. Catal. *264*, 77–87.

63. Hemelsoet, K., Nollet, A., Vandichel, M., Lesthaeghe, D., Van Speybroeck, V., and Waroquier, M. (2009). The Effect of Confined Space on the Growth of Naphthalenic Species in a Chabazite-Type Catalyst: A Molecular Modeling Study. ChemCatChem *1*, 373–378.

64. Hemelsoet, K., Nollet, A., Van Speybroeck, V., and Waroquier, M. (2011). Theoretical simulations elucidate the role of naphthalenic species during methanol conversion within H-SAPO-34. Chem. Eur J. *17*, 9083–9093.

65. Chen, J., Li, J., Wei, Y., Yuan, C., Li, B., Xu, S., Zhou, Y., Wang, J., Zhang, M., and Liu, Z. (2014). Spatial confinement effects of cage-type SAPO molecular sieves on product distribution and coke formation in methanol-to-olefin reaction. Catal. Commun. *46*, 36–40.

66. O'Malley, P.J., and Dwyer, J. (1988). Ab-initio molecular orbital calculations on the siting of aluminium in the Theta-1 framework: Some general guidelines governing the site preferences of aluminium in zeolites. Zeolites *8*, 317–321.

Please cite this article in press as: Zhang et al., Water-assisted shape-selective production of ethene in methanol-to-olefins reaction on SAPO-34, Chem Catalysis (2024), https://doi.org/10.1016/j.checat.2024.101025

67. Chai, J.D., and Head-Gordon, M. (2008). Long-range corrected hybrid density functionals with damped atom-atom dispersion corrections. Phys. Chem. Chem. Phys. *10*, 6615–6620.

68. Frisch, M.J., T, G.W., Schlegel, H.B., Scuseria, G.E., Robb, M.A., Cheeseman, J.R., Scalmani, G., Barone, V., Mennucci, B., Peters son, G.A., et al. (2010). Gaussian 09, Revision B.01 (Gaussian, Inc.).

69. Ghysels, A., Verstraelen, T., Hemelsoet, K., Waroquier, M., and Van Speybroeck, V. (2010). TAMkin: A Versatile Package for Vibrational Analysis and Chemical Kinetics. J. Chem. Inf. Model. *50*, 1736–1750.

70. Parr, R.G. (1989). Density Functional Theory of Atoms and Molecules (Oxford University Press).

71. Pino-Rios, R., Yañez, O., Inostroza, D., Ruiz, L., Cardenas, C., Fuentealba, P., and Tiznado, W. (2017). Proposal of a simple and effective local reactivity descriptor through a topological analysis of an orbital-weighted fukui function. J. Comput. Chem. *38*, 481–488.

72. Pino-Rios, R., Inostroza, D., Cárdenas-Jirón, G., and Tiznado, W. (2019). Orbital-Weighted Dual Descriptor for the Study of Local Reactivity of Systems with (Quasi-) Degenerate States. J. Phys. Chem. A *123*, 10556–10562.

73. Lu, T., and Chen, F. (2012). Multiwfn: a multifunctional wavefunction analyzer. J. Comput. Chem. *33*, 580–592.